J. Fluid Mech. (1995), *vol.* 299, *pp.* 1–15

Transport processes in periodic porous media

By R. B. SAEGER, L. E. SCRIVEN AND H. T. DAVIS

Department of Chemical Engineering and Materials Science, University of Minnesota, Minneapolis, MN 55404, USA

(Received 28 April 1992 and in revised form 12 May 1995)

The Stokes equation system and Ohm's law were solved numerically for fluid in periodic bicontinuous porous media of simple cubic (SC), body-centred cubic (BCC) and face-centred cubic (FCC) symmetry. The Stokes equation system was also solved for fluid in porous media of SC arrays of disjoint spheres. The equations were solved by Galerkin's method with finite element basis functions and with elliptic grid generation. The Darcy permeability k computed for flow through SC arrays of spheres is in excellent agreement with predictions made by other authors. Prominent recirculation patterns are found for Stokes flow in bicontinuous porous media. The results of the analysis of Stokes flow and Ohmic conduction through bicontinuous porous media were used to test the permeability scaling law proposed by Johnson, Koplik & Schwartz (1986), which introduces a length parameter Λ to relate Darcy permeability k and the formation factor F. As reported in our earlier work on the SC bicontinuous porous media, the scaling law holds approximately for the BCC and FCC families except when the porespace becomes nearly spherical pores connected by small orifice-like passages. We also found that, except when the porespace was connected by the small orifice-like passages, the permeability versus porosity curve of the bicontinuous media agrees very well with that of arrays of disjoint and fused spheres of the same crystallographic symmetry.

1. Introduction

Flow through bundles of tubes (von Brackel 1975), cubic arrays of disjoint spheres (Hasimoto 1959; Sørenson & Stewart 1974; Sangani & Acrivos 1982; Zick & Homsy 1982) and cubic arrays of interpenetrating spheres (Larson & Higdon 1988) has been analysed extensively in order to understand flow though porous media. The pore–solid surfaces in a bundle of tubes lack interconnected porespace and Gaussian curvature. Interpenetrating spheres have Gaussian curvature singularities along the seams between spheres. Natural porous media, on the other hand, frequently have porespace in which the curvature of the surfaces has become continuously distributed through such processes as sintering, cementation or diagenesis. It is thus of interest to examine flow in families of porous media in which the curvature distribution is continuous and to compare the results with flow in disjoint and interpenetrating arrays of spheres. In this paper we report such a study.

The model porous media we examine are periodic, bicontinuous (continuously connected porespace and continuously connected solid matrix), have pore surfaces with uniform mean curvature, and have simple cubic (SC), body-centred cubic (BCC) or face-centred cubic (FCC) symmetry. For a given symmetry, a family of porous media of varying porosity is generated by varying the mean curvature. These three symmetry classes are among the families of triply periodic bicontinuous structures with uniform interface mean curvature that were computed by Anderson *et al.* (1990).

In what follows we report numerical solutions of the Stokes equations for steady flow and Ohm's law for steady conduction of a fluid in the bicontinuous porous media. The permeability k and the effective conductivity σ are also presented. In a previous study (Saeger, Scriven & Davis 1991) of the SC family, we tested Johnson, Koplik & Schwartz's (1986) conjectured scaling law that

$$M \equiv \frac{8\sigma k}{\sigma_f \Lambda^2} \approx 1, \tag{1}$$

with σ_f the conductivity of the bulk fluid and Λ a length parameter defined by

$$\Lambda = 2\int_V (\nabla\psi)^2 \,\mathrm{d}V / \int_S (\nabla\psi)^2 \,\mathrm{d}S, \tag{2}$$

where ψ is the electric potential in the porespace during steady conduction, and S is the surface and V the volume of the porespace. The validity and limitations of (1) are explored further in a subsequent section.

Pore segments represented by hyperboloids of revolution (Rajagopalan & Tien 1976) are used in the analysis of transport through periodic bicontinuous porous media in the curvature range where porespace consists of almost spherical pore bodies connected by tiny sharply converging–diverging necks.

2. Interfaces of prescribed mean curvature

Unit cells of members of the SC, BCC and FCC families are shown in figures 1–3 for various mean curvatures H, where $H = [1/R_1 + 1/R_2]/2$. R_1 and R_2 are the principal radii of curvature and are taken to be positive for curvature into the solid. The curvature is given herein in units of $1/a$, where a is the half-length of the edge of a unit cell. Also, the porosity Φ of the porespace is plotted as a function of curvature in figures 1–3. The coordinates of the pore surfaces were computed by Anderson *et al.* (1990) for these families. In the SC family (see figure 1) at zero mean curvature the porespace and solid matrix are each identical sample-spanning labyrinths and the interface between them is Schwarz's periodic minimal surface (Schwarz 1890). The positive curvature branch of the family of constant mean curvature interfaces loops through a turning point and then terminates at $H = 1$, where the continuous solid matrix becomes a SC packing of spheres making point contacts – a SC bead pack. The negative curvature branch loops through a complementary turning point and terminates at $H = -1$, where the continuous porespace becomes a SC packing of bubbles making point contacts – a SC inclusion array, or a bubble pack. Just short of that the porespace consists of almost spherical pore bodies connected by tiny sharply converging–diverging necks. The dashed curves indicate interfaces of prescribed mean curvature H for which the solid matrix and porespace are no longer both continuous. The dashed curve on the right terminates at the SC bead pack limit ($H = 1$, $\Phi = 1 - \pi/6 \approx 0.476$). At mean curvature $H > 1$ along the dashed curve the porespace is the space between SC arrays of disjoint solid spheres. The dashed curve on the left terminates at the SC bubble pack limit ($H = -1$, $\Phi = \Pi/6 \approx 0.524$). At mean curvature $H < -1$ along the dashed curve the porespace is an SC array of isolated spherical bubbles in a continuous solid matrix.

In the BCC family (see figure 2), the zero mean curvature interface defines a porespace of porosity $\Phi = 0.464$. The BCC bead pack limit is at $H = 2/\sqrt{3}$, $\Phi = 1 - \pi\sqrt{3}/8 \approx 0.320$ and the dashed curve on the right is the solution branch where the porespace is that between a BCC array of solid spheres. At the bubble pack limit

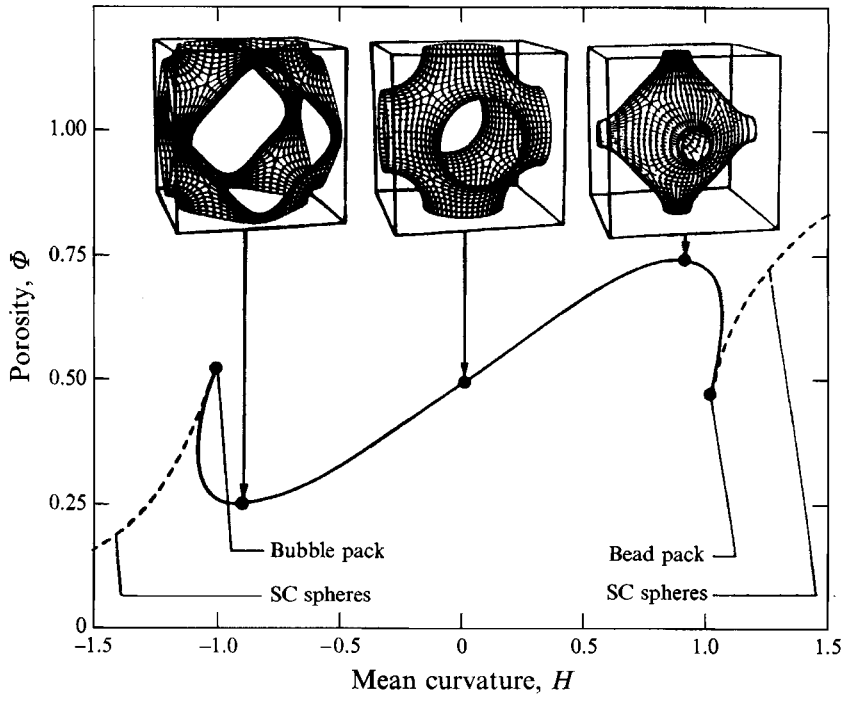

FIGURE 1. Solid–porespace interfacial mean curvature H *vs.* porosity Φ of simple dubic (SC) porous media. Unit cells of bicontinuous media: $H = -0.8987$, $\Phi = 0.25$ (left), $H = 0$, $\Phi = 0.5$ (centre), $H = 0.8987$, $\Phi = 0.75$ (right).

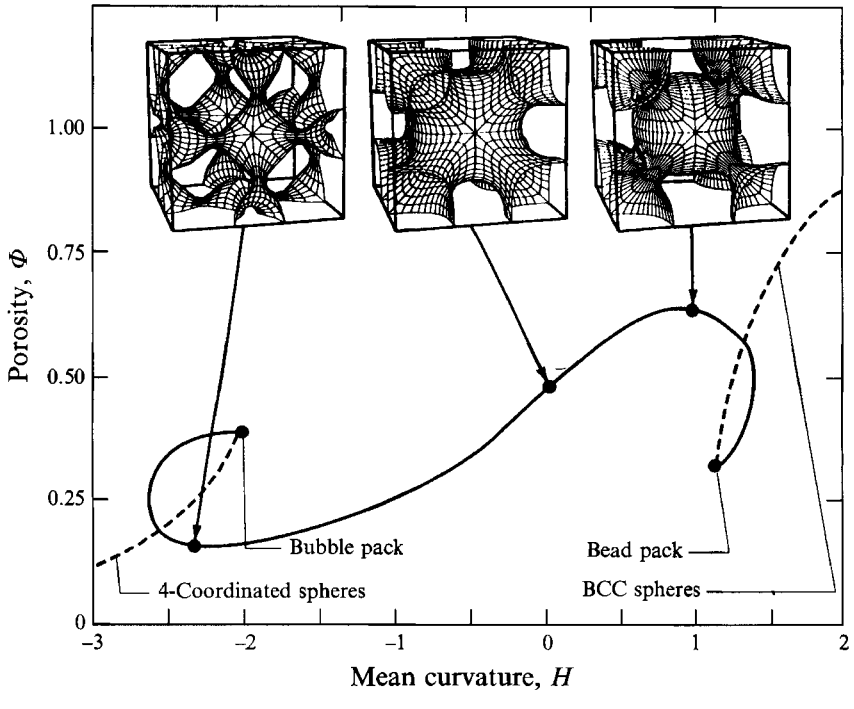

FIGURE 2. Solid-porespace interfacial mean curvature H *vs.* porosity Φ of body-centred cubic (BCC) porous media. Units cells of bicontinuous media: $H = -2.26$, $\Phi = 0.143$ (left), $H = 0$, $\Phi = 0.464$ (centre), $H = 0.97$, $\Phi = 0.643$ (right).

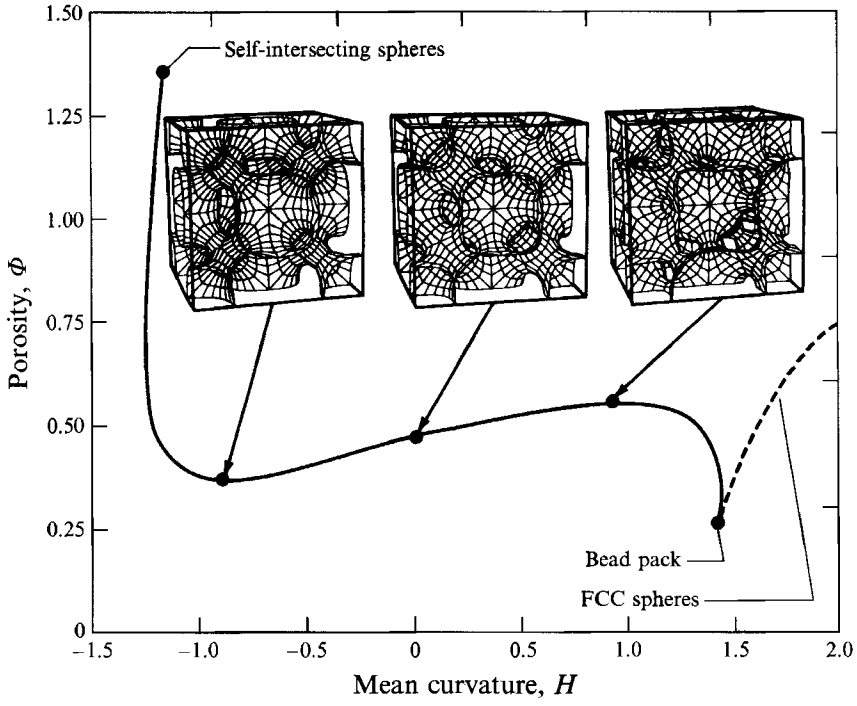

FIGURE 3. Solid-porespace interfacial mean curvature H *vs.* porosity Φ of face-centred cubic (FCC) porous media. Unit cells of bicontinuous media: $H = -0.89$, $\Phi = 0.363$ (left), $H = 0$, $\Phi = 0.468$ (centre), $H = 0.95$, $\Phi = 0.561$ (right).

($H = -2$, $\Phi = \pi/8 \approx 0.393$), and at the solution branch where the porespace consists of isolated spherical bubbles ($H < 2$), the bubbles are in a four-coordinated 'wrapped package' array (Schoen 1970).

In the FCC family (see figure 3), the positive curvature terminus of the bicontinuous solution branch is the FCC bead pack limit ($H = \sqrt{2}$, $\Phi = 1 - \pi\sqrt{2}/6 \approx 0.260$). Beyond this curvature the porespace is that between a FCC array of solid spheres. Self-intersecting interface surfaces occur on the negative curvature solution branch. They start at $H \approx -1.23$, $\Phi \approx 0.66$, and they continue to occur up to the terminus of the negative curvature solution branch at $H = -1.16$, $\Phi = 1.36$, where the porespace consists of self-intersecting spheres. In the analysis by Anderson *et al.* (1990) a fraction of the porespace is double-counted when interface surfaces overlap. Porosity Φ is therefore artificially high, and even exceeds unity in some cases. Transport in porous media with self-intersecting interface surfaces was not analysed in this work.

3. Analysis of Stokes flow

Creeping flow within the fluid-filled porespace is that of a single-phase Newtonian fluid of viscosity μ. The field velocity $\boldsymbol{u}$ and pressure p were obtained by solving the Stokes flow equation system $\mu\nabla^2\boldsymbol{u} - \nabla p = \boldsymbol{0}$, $\nabla\cdot\boldsymbol{u} = 0$ on the unit cell. Uniform pressures were imposed on the opposed inflow face and outflow face. Appropriate symmetry conditions were imposed on all six faces, and the no-slip and no-penetration boundary condition $\boldsymbol{u} = \boldsymbol{0}$ was applied at the interface between fluid and solid. Given the symmetries of the system, the solution was computed only on a Stokes flow primitive cell, which was one-sixteenth of the unit cell. The Stokes system was solved

within the Stokes flow primitive cell by Galerkin's method with finite element basis functions (Strang & Fix 1973). The velocity $\boldsymbol{u}$ and pressure p were expanded in triquadratic basis functions ϕ^t and trilinear basis functions Ψ^k respectively: the numerical details of computations are given elsewhere (Saeger 1991; Saeger, Davis & Scriven 1990).

Once the velocity and pressure fields were obtained, the Darcy permeability k was computed from Darcy's law (Darcy 1856). For the isotropic porous media shown in figures 1–3, this law is $\mu U = -k\Delta p/2a$, where μ is the fluid viscosity, and Δp is the pressure difference between the outflow and inflow faces of the unit cell, and the superficial velocity U is the velocity at either the inflow or outflow face.

4. Analysis of Ohmic conduction

The steady-state distribution of potential ψ within a porespace filled with static fluid was obtained by solving the Ohmic conduction boundary value problem, i.e the Laplace equation $\nabla^2\psi = 0$, on the unit cell with uniform potentials ψ_i, and ψ_o imposed on the opposed influx face and outflux face, and vanishing current flux required on all four lateral faces as well as at the interface between conductive fluid and non-conductive solid. The potential ψ that satisfies the Laplace equation within the unit cell has the same sixteen-fold symmetry as the Stokes flow velocity and pressure fields. Thus the primitive cells for Stokes flow and Ohmic conduction are identical.

As was done for the Stokes system, the Laplace equation was solved within its primitive cell by Galerkin's method with finite element basis functions. The potential ψ was expanded in the same triquadratic basis functions ϕ^t used for velocity. The porespace was divided into the same finite elements previously used to analyse the Stokes system. For numerical details see Saeger (1991) or Saeger *et al.* (1990).

Once the potential distribution within the Ohmic conduction primitive cell was found, the conductivity ratio, $\sigma/\sigma_f \equiv 1/F = (\int \boldsymbol{n}\cdot\nabla\psi \, dS)/a(\psi_i - \psi_o)$, was evaluated over the influx or outflux face of the unit cell. F is the so-called formation factor. The length parameter Λ was evaluated from (2).

5. Flow and conduction in hyperboloid pore segments

In the Galerkin/finite element analysis of conduction and flow in periodic bicontinuous porous media, the cost of adequate numbers of basis functions to represent conduction and flow with adequate accuracy prevented us from examining the details of flow and transport of the SC and BCC near the bubble pack limits (see figures 1 and 2) where the narrowing necks between nearly spherical pore bodies become the chief resistance to flow and conduction. In our earlier work (Saeger *et al.* 1991) we introduced an approximation in which we simply neglect resistances to flow and conduction in the pore bodies, and fit pore necks by the method of least squares to sharply converging–diverging hyperboloids of revolution. As seen in figure 4 the fit is quite good when the necks are small.

The total pressure drop Δp across a converging–diverging pore segment (Happel & Brenner 1983) is

$$\Delta p = \frac{3q\mu \sin^3\theta}{R^3(1+2\cos\theta)(1-\cos\theta)^2}, \tag{3}$$

where q is the volumetric flow rate through the pore segment, R is the minimum pore throat radius, and $0 < \theta < \pi/2$ is the angle of the asymptote of the generating

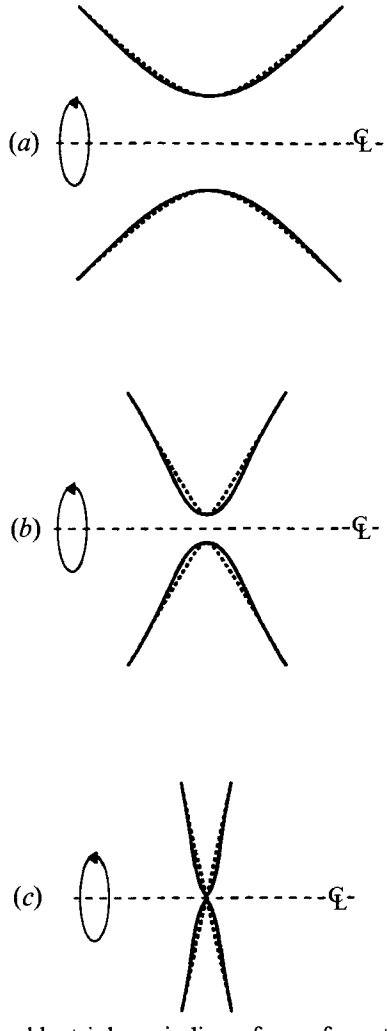

FIGURE 4. Pore segments defined by triply periodic surfaces of constant mean curvature H and simple cubic symmetry (——), and their least-squares fit to hyperboloids of revolution (· · · · · ·): (*a*) mean curvature $H = -0.8987$, porosity $\Phi = 0.25$; (*b*) $H = -1.0750$, $\Phi = 0.375$; (*c*) $H = -1.05$, $\Phi = 0.475$.

hyperbola. A unit cell of the SC porous medium (see figure 1) contains one converging–diverging pore segment, and $q \equiv 4a^2U$. BCC media (see figure 2) contain two converging–diverging pore segments per unit cell, but half the total pressure drop across the unit cell is seen by each one. Thus the Darcy permeability k of a single hyperboloid pore segment is

$$k = \frac{R^3(1+2\cos\theta)(1-\cos\theta)^2}{6a \qquad \sin^3\theta}. \tag{4}$$

The solution of Laplace's equation with non-conducting pore walls, and fixed potentials ψ_i, ψ_o at the influx and outflux sections is (Moon & Spencer 1961)

$$\psi = \tfrac{1}{2}(\psi_i+\psi_o)+\tfrac{1}{2}(\psi_i-\psi_o)\tan^{-1}(\sinh\xi), \tag{5}$$

where $\xi \to \infty$ is the influx section, $\xi \to -\infty$ is the outflux section, and the coordinate surface $\xi = 0$ is a circular disk that bisects the pore segment at its throat. The total

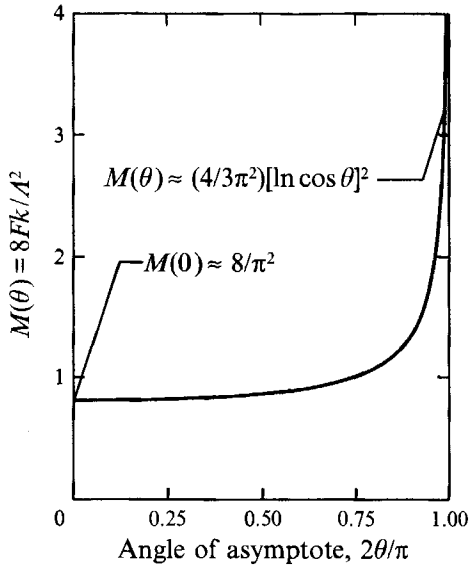

FIGURE 5. Permeability rates M versus asymptotic angle $0 < \theta < \pi/2$ of hyper-boloid pore segments, equation (8). As $\theta \to 0$, $M \to 8/\pi^2 \approx 0.8106$. As $\theta \to \pi/2$, $M \approx (4/3\pi^2)[\ln\cos\theta]^2 \to \infty$.

current flux can be evaluated at this throat, and the formation factor F of a single pore segment is

$$F = \frac{a\sin\theta}{R(1-\cos\theta)}. \tag{6}$$

The length parameter Λ from (1) is then

$$\Lambda = \frac{\pi R}{\ln[(1+\sin\theta)/\cos\theta]}\left(\frac{1-\cos\theta}{1+\cos\theta}\right)^{1/2}. \tag{7}$$

Thus for a single pore segment the permeability ratio M defined in (1) depends only on the angle θ:

$$M = 8[F][k][\Lambda]^{-2} = \frac{4}{3\pi^2}(1+2\cos\theta)(1+\cos\theta)\left\{\frac{\ln[(1+\sin\theta)/\cos\theta]}{\sin\theta}\right\}^2. \tag{8}$$

The ratio M is plotted versus θ in figure 5. This figure shows that the conjecture of Johnson *et al.* (1986) will fail for porespace connected by small orifices, although for $0 < \theta < 80°$ the quantity M lies between 0.8 and 1.5.

6. Results

6.1. *Permeability of SC arrays of spheres*

The Darcy permeability k obtained from the Galerkin/finite element analysis of the Stokes equation system in SC arrays of spheres is shown in figure 6. These results are also reported as the Stokes drag coefficient $C_D = F_d/6\pi\mu r U$, where the sphere radius $r = 1/H$, and F_d is the drag force on the sphere. The drag coefficient and permeability are simply related to each other, namely, $k = (2a)^3/(6\pi r C_D)$, where $(2a)^3$ is the volume of the unit cell. The inlet and outlet mass flow rates through the Stokes-flow primitive cell computed by the Galerkin/finite element method agreed to eight decimal places. The pressure force applied across the primitive cell, and the traction force $\int \boldsymbol{n}\cdot\boldsymbol{T}\,\mathrm{d}S$ at

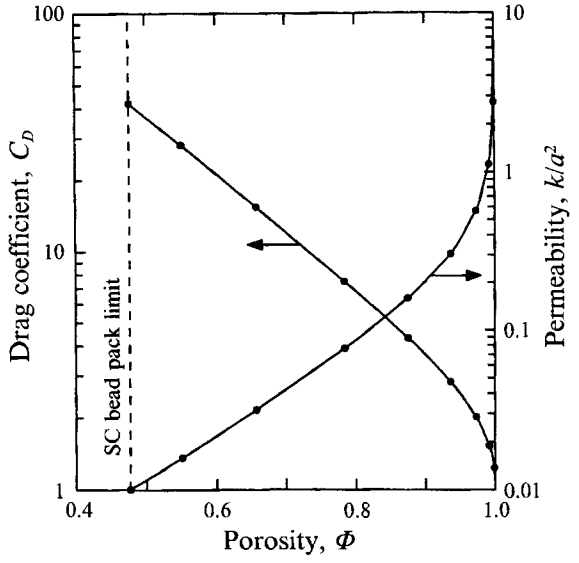

FIGURE 6. Curves show literature values (Zick & Homsy 1982; Sangani & Acrivos 1982; Larson & Higdon 1988) compared with our Galerkin/finite element predictions (solid circles) of the Stokes drag coefficient C_D and Darcy permeability k/a^2 of SC arrays of spheres.

c.f.	H	Φ	k/a^2	F	Λ/a	M
SC	−1.0625	0.312	2.67×10^{-5}	3.20×10^{1}	8.25×10^{-2}	1.00
SC	−0.8987	0.250	4.05×10^{-4}	1.34×10^{1}	2.13×10^{-1}	0.955
SC	−0.3115	0.375	5.23×10^{-3}	4.67×10^{0}	4.40×10^{-1}	1.01
SC	0.0000	0.500	1.35×10^{-2}	3.00×10^{0}	5.67×10^{-1}	1.01
SC	0.3115	0.625	2.82×10^{-2}	2.12×10^{0}	7.07×10^{-1}	0.960
SC	0.8987	0.750	5.62×10^{-2}	1.56×10^{0}	9.40×10^{-1}	0.792
SC	1.0750	0.625	2.61×10^{-2}	1.96×10^{0}	6.45×10^{-1}	0.983
SC	1.0375	0.515	1.28×10^{-2}	2.56×10^{0}	4.10×10^{-1}	1.56
BCC	−2.2600	0.143	3.94×10^{-5}	3.11×10^{1}	9.84×10^{-2}	1.01
BCC	−1.1300	0.218	7.54×10^{-4}	9.24×10^{0}	2.34×10^{-1}	1.01
BCC	0.0000	0.463	6.02×10^{-3}	3.22×10^{0}	3.88×10^{-1}	1.03
BCC	0.3625	0.560	1.05×10^{-2}	2.43×10^{0}	4.54×10^{-1}	0.989
BCC	0.9700	0.643	1.62×10^{-2}	1.91×10^{0}	5.39×10^{-1}	0.855
BCC	1.3800	0.560	9.51×10^{-3}	2.24×10^{0}	4.40×10^{-1}	0.880
BCC	1.4000	0.530	7.57×10^{-3}	2.36×10^{0}	4.18×10^{-1}	0.819
BCC	1.3800	0.460	4.57×10^{-3}	2.79×10^{0}	3.31×10^{-1}	0.930
FCC	−1.1790	0.468	1.6×10^{-4}	9.8×10^{0}	1.1×10^{-1}	1.1
FCC	−0.8900	0.363	5.6×10^{-4}	6.5×10^{0}	1.6×10^{-1}	1.1
FCC	−0.4450	0.406	1.3×10^{-3}	4.6×10^{0}	2.1×10^{-1}	1.1
FCC	0.0000	0.468	2.4×10^{-3}	3.4×10^{0}	2.5×10^{-1}	1.0
FCC	0.4750	0.531	3.9×10^{-3}	2.7×10^{0}	2.9×10^{-1}	0.98
FCC	0.9500	0.561	4.9×10^{-3}	2.4×10^{0}	3.2×10^{-1}	0.91
FCC	1.2640	0.531	4.1×10^{-3}	2.4×10^{0}	3.0×10^{-1}	0.86
FCC	1.4600	0.374	1.2×10^{-3}	3.8×10^{0}	1.8×10^{-1}	1.0

c.f. ≡ crystallographic family.

TABLE 1. Predictions of viscous flow and charge transport properties of bicontinuous porous media, calculated by means of Galerkin's method and finite element basis functions (sufficient in number that all reported digits are significant).

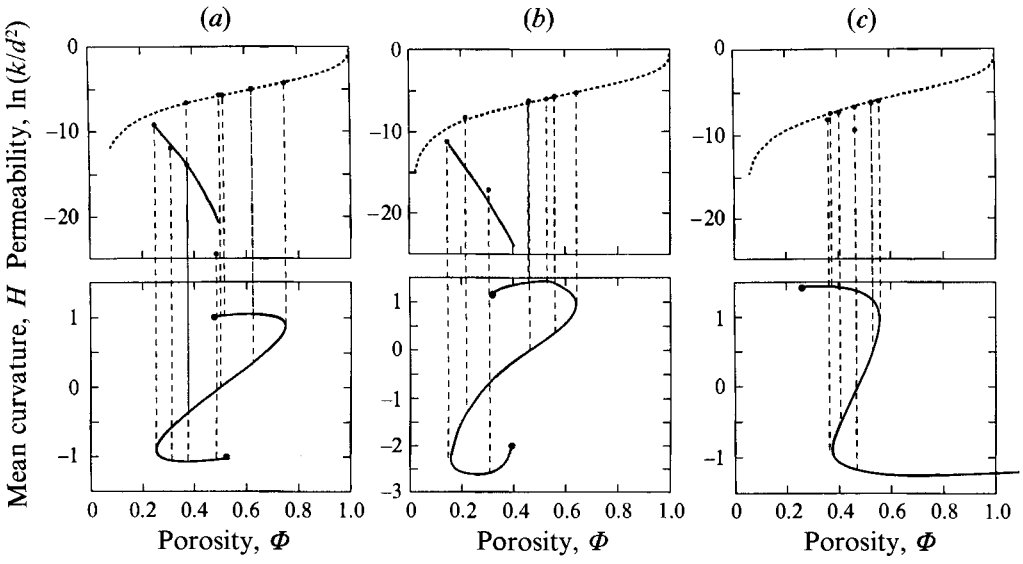

FIGURE 7. Darcy permeability k/d^2 and mean curvature *vs.* porosity Φ. Galerkin/finite element results for bicontinuous porous media (●) are compared with results for arrays of discrete, contacting and overlapping spheres (dashed curves, Larson & Higdon 1988), and with predictions of the hyperboloid model (solid curves in the permeability plots). (*a*) SC ($d = 2a$), (*b*) BCC ($d = a\sqrt{3}$), (*c*) FCC ($d = a\sqrt{2}$).

the spherical solid–porespace interface were compared. These values agreed to within 0.02% at the SC bead pack (close-packed) limit ($H = 1$, $\Phi = 1 - \pi/6 \approx 0.4764$), and to within 1.8% at the highest porosity analysed ($H = 8.060$, $\Phi = 0.9990$).

As indicated by figure 6, the Galerkin/finite element results show excellent agreement with literature values. At $H = 8.060$, $\Phi = 0.9990$, the drag coefficient C_D differed from the value obtained from the boundary-element analysis of Zick & Homsy (1982) by 2.3%. Otherwise these two sets of values differed by less than 0.35%. As porosity $\Phi \to 1$, velocity gradients in the vicinity of the sphere's surface become large. The Galerkin/finite element method required more basis functions than were affordable to accurately resolve these gradients. Thus disagreement with literature values and errors in the total force balance were larger at this limit than at the bead pack limit. Fortunately, as $\Phi \to 1$, the analysis of the Stokes equation system by Hasimoto (1959) becomes more accurate and is cheaper so that the effort required to perform Galerkin/finite element computations becomes unnecessary.

6.2. *Permeability of bicontinuous porous media*

The Darcy permeability k of SC, BCC and FCC bicontinuous porous media obtained from the Galerkin/finite element analysis of the Stokes equation system is listed in table 1, and is shown in the upper portion of figure 7(*a–c*). In these figures the units of permeability, d^2, are those used by Larson & Higdon (1988), i.e. $d = 2a$ for SC, $d = a\sqrt{3}$ for BCC and $d = a\sqrt{2}$ for FCC. The results of this work were compared with those of Larson & Higdon (1988), who analysed Stokes flow through discrete, contacting and overlapping spheres in SC, BCC and FCC arrays. For porespaces near the bubble pack limits of the SC and BCC families, the Galerkin/finite element results were compared with those of the hyperboloid pore segment model, equation (4).

Like the Galerkin/finite element analysis of Stokes flow in SC arrays of spheres, mass balances across the primitive cell closed to within eight decimal places for SC,

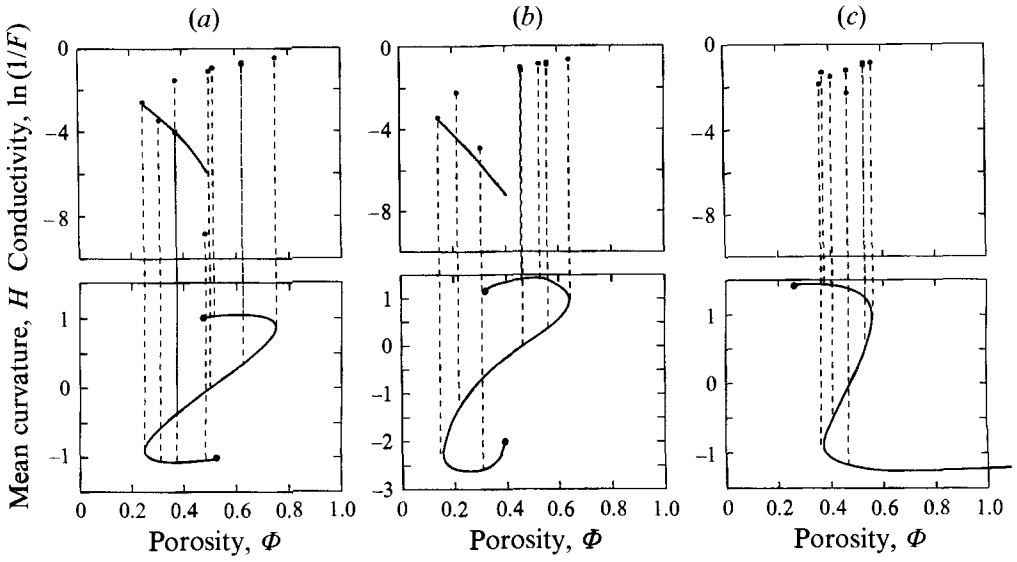

FIGURE 8. Ohmic conductivity $1/F$ and mean curvature *vs.* porosity Φ. Galerkin/finite element results for bicontinuous porous media (●) are compared with the hyperboloid model (solid curves in the conductivity plots). (*a*) SC, (*b*) BCC, (*c*) FCC.

BCC and FCC bicontinuous media. For porespaces other than the closest approaches to bubble pack limits, e.g. $H = -1.0375$, $\Phi = 0.485$ for SC and $H = -2.5575$, $\Phi = 0.307$ for BCC, the agreement between applied pressure forces and computed traction forces was between 0.01% and 1.8%. As mentioned in §5, the accuracy of affordable basis functions fell as the SC and BCC bubble pack limits were approached.

For mean curvature H greater than the value at minimum porosity of each crystallographic family, permeability is a unique, increasing function of porosity Φ, as it is for the media used by Larson & Higdon (1988). In the SC family (see figure 7*a*), the worst agreement between the permeability values obtained for these two types of media is 15% ($H = 0$, $\Phi = 0.5$); the best is 0.31% at $H = 1.0375$, $\Phi = 0.515$. In the BCC family (see figure 7*b*), the worst is 39% ($H = -1.13$, $\Phi = 0.218$), and the best is 0.34% ($H = 1.38$, $\Phi = 0.46$). In the FCC family (see figure 7*c*), the worst is 44% ($H = -0.89$, $\Phi = 0.363$), and the best is 2.12% ($H = 1.46$, $\Phi = 0.374$). These trends are expected because the porespaces used in this work and those of Larson & Higdon (1988) are identical at the bead pack limit of each family.

As the SC and BCC bubble pack limits were approached, permeability k fell rapidly to zero. In the SC family, the values obtained from the Galerkin/finite element results and the hyperboloid pore segment model, (4), agree to within 25% ($H = -0.8987$, $\Phi = 0.25$), and 19% ($H = -1.075$, $\Phi = 0.375$). Nearer the SC bubble pack limit ($H = -1.0375$, $\Phi = 0.485$), where the accuracy of the Galerkin/finite element results is poor, the values obtained by the two methods differ by two orders of magnitude. In the BCC family, the two methods agree to within 27% ($H = -2.26$, $\Phi = 0.147$) and 183% ($H = -2.5575$, $\Phi = 0.307$). As the overlapping porespaces were approached in the FCC family, permeability fell less rapidly than in the SC and BCC families.

6.3. *Conductivity of bicontinuous porous media*

The formation factor F of SC, BCC and FCC bicontinuous porous media obtained from the Galerkin/finite element analysis of the Laplace equation system is listed in table 1, and the conductivity $1/F$ is shown in the upper portion of figure 8(*a–c*). Influx

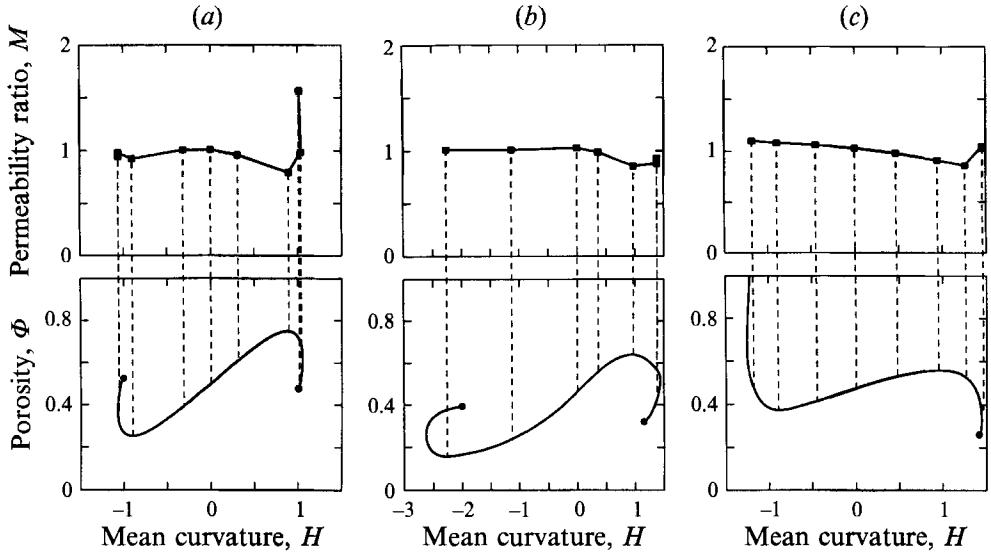

FIGURE 9. Permeability ratio $M \equiv 8Fk/\Lambda^2$ of bicontinuous porous media. Darcy permeability k, formation factor F, and the length parameter Λ are obtained from Galerkin/finite element analysis of Stokes flow and Ohmic conduction. (*a*) SC, (*b*) BCC, (*c*) FCC.

and outflux electric currents in the porespace agreed typically to within 0.4% for SC, 0.03% for BCC, and 0.5% for FCC media. Agreement was to within 40% for porespaces nearest the bubble pack limits of the SC ($H = -1.0375$, $\Phi = 0.485$) and BCC ($H = -2.5575$, $\Phi = 0.307$) families. In this region of porespace, where the accuracy of affordable basis functions fell, Galerkin/finite element results were compared with those of the hyperboloid pore segment model, equation (6).

The conductivity $1/F$ showed a dependence upon porosity Φ, or mean curvature H, like that of the Darcy permeability k. At mean curvatures greater than the value at minimum porosity, conductivity is a unique, increasing function of porosity Φ. As the SC and BCC bubble pack limits were approached, conductivity fell rapidly to zero. As the overlapping porespaces were approached in the FCC family, conductivity fell less rapidly than in the SC and BCC families. In the SC family, the conductivity $1/F$ obtained from the Galerkin/finite element results and the hyperboloid pore segment model (6), agree to within 4.0% at $H = -0.8987$, $\Phi = 0.25$, and 11% at $H = -1.075$, $\Phi = 0.375$. At $H = -1.0375$, $\Phi = 0.485$, the hyperboloid value is 20 times larger than the Galerkin/finite element value. In the BCC family, results of these two methods agree to within 9.3% at $H = -2.26$, $\Phi = 0.147$, and 79% at $H = -2.5575$, $\Phi = 0.307$.

6.4. *Characteristic length and permeability ratio of bicontinuous porous media*

The permeability ratio M of SC, BCC and FCC bicontinuous porous media obtained from Galerkin/finite element results is listed in table 1, and are plotted versus mean curvature H in the upper portion of figure 9(*a–c*). The results shown in these figures are those where the affordable sets of basis functions yielded accuracy in M to three significant figures for SC and BCC media, and two for FCC media. At zero mean curvature, $M = 1.01$ for SC, $M = 1.03$ for BCC and $M = 1.02$ for FCC media. In all three families there are local minima in M at the maximum porosity of the positive mean curvature solution branch. As the SC solid sphere limit ($H = 1$) is approached, the permeability ratio M climbs abruptly as the porespace loses all resemblance to

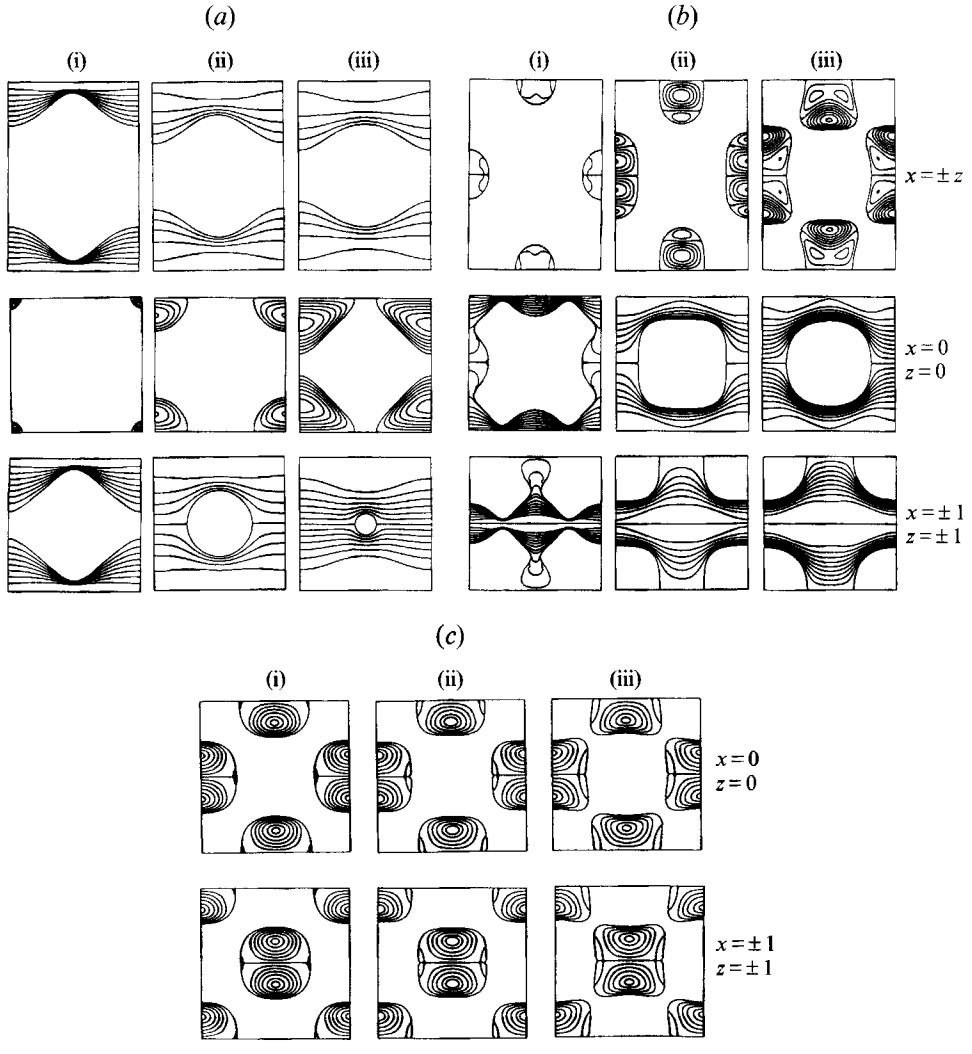

FIGURE 10. Stokes-flow streamlines at symmetry planes of bicontinuous porous media (*a*) SC: (i) $H = -0.8987$, $\Phi = 0.25$; (ii) $H = 0$, $\Phi = 0.5$; (iii) $H = 0.8987$, $\Phi = 0.75$. (*b*) BCC: (i) $H = -2.26$, $\Phi = 0.143$; (ii) $H = 0$, $\Phi = 0.464$; (iii) $H = 0.97$, $\Phi = 0.643$. (*c*) FCC: (i) $H = -0.89$, $\Phi = 0.363$; (ii) $H = 0$, $\Phi = 0.468$; (iii) $H = 0.95$, $\Phi = 0.561$.

converging–diverging tubes, and the solid matrix degenerates to a bead pack. In the SC and BCC families there are shallow local minima in M at minimum porosity. On the negative curvature solution branch of all three families, as pore throats narrow, the permeability ratio M is approximately 1. As the disjoint bubble pack limit is approached the permeability and conductivity are well approximated by the hyperboloid pore segment model. Moreover, as the disjoint bubble pack limit is approached in the SC and BCC families, the angle θ of the asymptote of the approximating hyperboloid segment approaches $\pi/2$ and so, from (8), it follows that $M \approx (4/3\pi^2)[\ln\cos\theta]^2$ as $\theta \to \pi/2$. Thus, as mentioned above, the scaling law of Johnson *et al.* (1986) ultimately fails. However, it is a good approximation except very near the disjoint bubble limit in the bicontinuous families studied here. In the SC family, θ is about 80° at a curvature $H = -1.05$ and porosity $\Phi = 0.475$ (see figure 4*c*),

and so the approximation begins to fail at this curvature and gets progressively worse as the disjoint bubble limit is approached. Porous polyurethane foams represent a class of practical materials well approximated by bubbles connected by orifices. Banavar & Johnson (1987), Banavar, Cieplak & Johnson (1988), and Kostek, Schwartz & Johnson (1992) have also reported cases for which the scaling law fails.

6.5. *Recirculation in bicontinuous porous media*

Streamlines, or level curves of the stream function A, were obtained for symmetry planes of the unit cell satisfying the impenetrability condition $\boldsymbol{n}\cdot\boldsymbol{u} = 0$. This was done by solving the elliptic equation $\nabla^2 A - \boldsymbol{n}\cdot(\nabla\times\boldsymbol{u}) = 0$ with appropriate boundary conditions for A imposed at edges of the symmetry plane. Galerkin's method with finite element basis functions was used on symmetry planes of the Stokes flow primitive cell. Symmetry conditions were then used to reconstruct recirculation patterns on these planes in the unit cell.

Streamlines on selected symmetry planes of SC, BCC and FCC bicontinuous porous media are shown in figure 10(*a–c*). The unit cells shown in figures 1–3 are the cube $-1 \leqslant x \leqslant 1$, $-1 \leqslant y \leqslant 1$, $-1 \leqslant z \leqslant 1$, and velocity $\boldsymbol{u}$ is in the negative y-direction at the opposed inflow and outflow faces. The equations of the symmetry planes in figure 10(*a–c*) are consistent with this assignment of coordinates. Prominent Stokes flow recirculation are indicated by the symmetry planes $x = 0$, $z = 0$ of the SC family, $x = \pm z$ of the BCC family and $x = 0$, $z = 0$, $x = \pm 1$, $z = \pm 1$ of the FCC family. The multiple recirculation cells of the BCC family (see figure 10*b*) are similar to those predicted for Stokes flow past sharp corners (see Moffatt 1964). The results of this work shed light on processes in porous media that are strongly influenced by diffusion, including chemical reactions and dispersion phenomena.

7. Discussion and conclusion

7.1. *Darcy permeability of Ohmic conductivity of biocontinuous porus media*

In each of the three crystallographic families (SC, BCC and FCC) of bicontinuous porous media, the dependence of both Darcy permeability k and conductivity $1/F$ on porosity Φ, or solid–porespace mean curvature H, shows three distinct regions of behaviour:

(i) *Curvature-independent region*

For interfacial mean curvature H greater than the value at minimum porosity Φ on the negative curvature solution branch, permeability k and conductivity $1/F$ are unique, increasing functions of porosity Φ. In this range of curvatures, permeability values agreed well with the results of Larson & Higdon (1988), suggesting that transport of momentum, and possibly charge is not strongly influenced by the presence of seams, i.e. concentrations of curvature at the solid–porespace interface.

(ii) *Pore-throat dominated region*

As the SC and BCC bubble pack limits are approached, permeability k and conductivity $1/F$ decay rapidly to zero, and are strong functions of porosity Φ or mean curvature H. All three crystallographic families show examples where transport properties can be double-valued at a given porosity Φ, a result absent from theoretical treatment of arrayed spheres.

(iii) *Transition region*

For SC, BCC and FCC bicontinuous media the transition between the curvature-independent region and the pore-throat dominated region (overlap region for FCC) is abrupt and occurs in the vicinity of minimum porosity Φ on the negative curvature solution branch.

7.2. *Permeability ratio of bicontinuous porous media*

The velocity field $\boldsymbol{u}$ of the Stokes system is generally rotational (i.e. $\nabla \times \boldsymbol{u} \neq 0$) whereas the electric field from Laplace's equation is irrotational (i.e. $\nabla \times \nabla\Phi = 0$). Thus, the general solution of the Stokes system cannot be derived from Laplace's equation for current flow. Nevertheless, the conjecture of Johnson *et al.* (1986) that $M \equiv 8Fk/\Lambda^2$ ($\Lambda \equiv 2\int(\nabla\Phi)^2\,dV/\int(\nabla\Phi)^2\,dS$), is approximately unity has been shown to hold for a wide variety of porous media, including those studied in this paper except where the transport resistance resides primarily in orifice-like throats. Avelleneda & Torquato (1991) have derived a rigorous expression for the relationship between F, k and relaxation times for transport in porous media from which $M = 1$ can be recovered as a special approximation. Further investigation along the lines of their work might enable one to anticipate cases in which F, k and Λ scale such that M deviates strongly from unity.

This research was supported by the Minnesota Supercomputer Institute, Cray Research, Inc., and the Center for Interfacial Engineering. One of us (R.B.S.) thanks Simon Brandon and Andrew Salinger for providing software that assisted in the graphical representation of flow streamlines.

REFERENCES

ANDERSON, D. M., DAVIS, H. T., SCRIVEN, L. E. & NITSCHE, J. C. C. 1990 Periodic surfaces of prescribed mean curvature. *Adv. Chem. Phys.* **77**, 337–396.

AVELLENADA, M. & TORQUATO, S. 1991 Rigorous link between fluid permeability, electrical conductivity, and relaxation times for transport in porous media. *Phys. Fluids* A **11**, 2529–2540.

BANAVAR, J. R., CIEPLAK, M. & JOHNSON, D. L. 1988 Surface conduction and length scales in porous media. *Phys. Rev.* B **37**, 7975–7978.

BANAVAR, J. R. & JOHNSON, D. L. 1987 Characteristic pore sizes and transport in porous media. *Phys. Rev.* B **35**, 7283–7286.

BRACKEL, J. VON 1975 Pore space models for transport phenomena in porous media: Review and evaluation with special emphasis on capillary treatment. *Powder Technol.* **11**, 205–236.

DARCY, H. P. G. 1856 *Les Fontaines Publiques de la Ville de Dijon.* Paris: Victor Dalmont.

HAPPEL, J. & BRENNER, H. 1983 *Low Reynolds Number Hydrodynamics*, 2nd rev. edn. Noordhoff.

HASIMOTO, H. 1959 On the periodic fundamental solution of the Stokes equations and their application to viscous flow past a cubic array of spheres. *J. Fluid Mech.* **5**, 317–328.

JOHNSON, D. L., KOPLIK, J. & DASHEN, R. 1987 Theory of dynamic permeability and tortuosity in fluid-saturated porous media. *J. Fluid Mech.* **176**, 379–402.

JOHNSON, D. L., KOPLIK, J. & SCHWARTZ, L. M. 1986 New pore-size paameter characterizing transport in porous media. *Phys. Rev. Lett.* **57**, 2564–2567.

KOSTEK, S., SCHWARTZ, L. M. & JOHNSON, D. L. 1992 Fluid permeability in porous media: comparison of electrical estimates with hydrodynamical calculations. *Phys. Rev.* B **45**, 186–195.

LARSON, R. E. & HIGDON, J. J. L. 1988 A periodic grain consolidation model of porous media. *Phys Fluids* A **1**, 38–46.

MEIJERINK, J. A. & VAN DER VORST, H. A. 1977 An iterative solution method for linear systems of which the coefficient matrix is a symmetric M-matrix. *Math. Comput.* **31**, 148–162.

MOFFATT, H. K. 1964 Viscous and resistive eddies near a sharp corner. *J. Fluid Mech.* **18**, 1–18.

MOON, P. & SPENCER, D. E. 1961 *Field Theory for Engineers*. D. Van Nostrand & Co.

RAJAGOPALAN, R. & TIEN, C. 1976 Trajectory analysis of deep bed filtration with the sphere-in-cell porous media model. *AIChE J.* **22**, 523–546.

SAAD, Y. & SCHULTZ, M. H. 1986 GMRES: A generalized minimum residual algorithm for solving nonsymmetric linear systems. *SIAM J. Sci. Statist. Comput.* 7, 417–424.

SAEGER, R. B. 1991 Equilibrium and transport processes in periodic microstructures. PhD dissertation, University of Minnesota.

SAEGER, R. B., DAVIS, H. T. & SCRIVEN, L. E. 1990 Adaptive elliptic grid generation for 3-D elemental structures. *University of Minnesota Supercomputer Institute Research Rep.* UMSI 90/73, April 1990.

SAEGER, R. B., SCRIVEN, L. E. & DAVIS, H. T. 1991 Flow, conduction, and a characteristic length in periodic bicontinuous porous media. *Phys. Rev.* A **44**, 5087–5090.

SANGANI, A. S. & ACRIVOS, A. 1982 Slow flow through a periodic array of spheres. *Intl J. Multiphase Flow* **8**, 343–360.

SCHOEN, A. H. 1970 Infinite periodic minimal surfaces without self-intersection. *NASA Tech. Note* TND-5541.

SCHWARZ, H. A. 1890 *Gesammelte Mathematische Abhandlungen*. Springer.

SØRENSON, J. P. & STEWART, W. E. 1974 Computation of forced convection in slow flow through ducts and packed beds – II. Velocity profile in a simple cubic array of spheres. *Chem. Engng Sci.* **29**, 819–825.

STRALEY, C., MATTESON, A., FENG, S., SCHWARTZ, L. M., KENYON, W. E. & BANAVAR, S. R. 1987 Magnetic resonance, digital image analysis, and permeability of porous media. *Appl. Phys. Lett.* **51**, 1146–1148.

STRANG, G. & FIX, G. 1973 *An Analysis of the Finite Element Method*. Prentice Hall.

ZICK, A. A. & HOMSY, G. M. 1982 Stokes flow through periodic arrays of spheres. *J. Fluid Mech.* **115**, 13–26.